Research Square

Preprints are preliminary reports that have not undergone peer review.
They should not be considered conclusive, used to inform clinical practice,
or referenced by the media as validated information.

Green Synthesis of Zinc Oxide Nanoparticles Using Castor Plant Extract and Their Antibacterial Activity Against Gram-Positive and Gram-Negative Bacteria

Ali Bahari
University of Mazandaran
Mohanad Ghulam
mohanadg.alzubaidi@uokufa.edu.iq
University of Kufa

Research Article

Keywords: Green synthesis, Castor extract, Zinc oxide nanoparticles, Optical band gap, Antibacterial activity

Posted Date: November 10th, 2026

DOI: https://doi.org/10.21203/rs.3.rs-11669027/v1

License: This work is licensed under a Creative Commons Attribution 4.0 International License.
Read Full License

Additional Declarations: No competing interests reported.

Green Synthesis of Zinc Oxide Nanoparticles Using Castor Plant Extract and Their Antibacterial Activity Against Gram-Positive and Gram-Negative Bacteria

Ali Bahari[1], Mohanad Ghulam Murad Alzubaidi[2, *]

[1]Department of Physics, Faculty of Basic Sciences, University of Mazandaran, Babolsar, Iran

[2]Department of Physics, Faculty of Dentistry, University of Kufa, Najaf, Iraq

***Corresponding author:** Mohanad Ghulam Murad Alzubaidi
E-mail: mohanadg.alzubaidi@uokufa.edu.iq

ORCID iDs
Mohanad Ghulam Murad Alzubaidi: 0009-0005-6807-3702
Ali Bahari: 0000-0002-4927-3144

Acknowledgments
The authors thank the Department of Physics, University of Mazandaran, and the University of Kufa for providing laboratory facilities and support for this work.

Green Synthesis of Zinc Oxide Nanoparticles Using Castor Plant Extract and Their Antibacterial Activity Against Gram-Positive and Gram-Negative Bacteria

Abstract

Zinc oxide nanoparticles (ZnO NPs) were synthesized through an environmentally friendly green methodology, using Ricinus communis (castor) seed extract as a bioreducing/capping agent at three zinc acetate concentrations (C1–C3: 0.01, 0.05 and 0.07 M), with the objective of fabricating a readily available antimicrobial nanomaterial while avoiding harmful traditional reagents. The samples were characterized by X-ray diffraction (XRD), Fourier transform infrared spectroscopy (FTIR), UV–Vis spectroscopy, field emission scanning electron microscopy with energy dispersive X-ray analysis (FE-SEM–EDX) and transmission electron microscopy (TEM). XRD confirmed the formation of the crystalline hexagonal wurtzite structure of ZnO with dominant (100), (002) and (101) peaks. FTIR revealed the Zn–O vibration band together with surface hydroxyl/adsorbed species characteristic of oxide NPs. FE-SEM and TEM images showed agglomerated nanocrystallites, with mean TEM sizes increasing from about 28 to 54 nm with precursor concentration. UV–Vis spectra revealed a wide band gap of about 3.1 eV.

The antibacterial activity showed clear, dose-dependent inhibition of Gram-negative Escherichia coli (E. coli) and Gram-positive Staphylococcus aureus (S. aureus); inhibition zones were absent at the lowest doses and increased up to about 22 mm for E. coli and 20 mm for S. aureus at 3 mg/mL. This is consistent with the commonly reported antibacterial mechanisms of ZnO NPs (reactive oxygen species (ROS)-induced stress, membrane disintegration and Zn^{2+}-mediated effects), indicating that castor-mediated ZnO NPs could be used as an antimicrobial material.

Keywords: Green synthesis, Castor extract, Zinc oxide nanoparticles, Optical band gap, Antibacterial activity

1 Introduction

In recent years, nanotechnology has become one of the most rapidly growing areas in science and promises to offer incredible solutions in medicine, microbiology, and environmental cleanup [1–3]. Nanoparticles (NPs) have attracted attention due to their specific features, including a high surface-to-volume ratio, increased reactivity and adjustable optical or catalytic properties, as well as their potential use in biomedical and antimicrobial sectors [4, 5]. However, both traditional chemical and physical methods of synthesis generally involve toxic reagents, high energy consumption and high temperatures that pose serious environmental health hazards [6, 7].

In order to overcome these drawbacks, green synthesis has received much attention as an environmental-friendly and sustainable replacement [8, 9]. In this method, the reduction and stabilization of metal precursor ions is carried out by plant extracts, microorganisms or natural biomolecules, under mild and non-toxic conditions resulting in the formation of nanoparticles [10, 11]. The importance of green synthesis lies not only in reducing environmental contamination but also in producing biocompatible, scalable and cost-effective products [12, 13].

Among natural resources, plants are regarded as effective nanofactories and present a large variety of phytochemicals like flavonoids, alkaloids, phenolics and terpenoids which aid in the formation of nanoparticles [14, 15]. These biomolecules are engaged in the reduction of metal ions and stabilize the resultant nanoparticles by surface functionalization [16]. Several reports have shown that plant-mediated ZnO NPs and Ag NPs possess strong antibacterial, antioxidant and anticancer capabilities [17, 18].

One such plant is Ricinus communis L. (castor plant), which grows widely in tropical and sub-tropical regions [19]. The seeds of R. communis are the source of castor oil, which has a high content of ricinoleic acid containing many carboxyl and hydroxyl groups which can act as reducing agents and cap nanoparticles [8, 9, 20]. Moreover, water and ethanolic extracts of Ricinus communis leaves, roots and seeds have been used in the production of metal and metal oxide nanoparticles, including Ag, Fe_2O_3, ZnO NPs [21, 22]. These biogenic nanoparticles exhibit considerable antimicrobial efficacy towards Gram-positive and Gram-negative microorganisms, including Staphylococcus aureus and Escherichia coli [8, 23].

The antibacterial activity of these green-synthesised nanoparticles is considered multifaceted: the formation of reactive oxygen species (ROS), destruction of bacterial membranes and cytoplasmic leakage and interference with enzymatic pathways [16, 17, 23]. In addition, phytochemical capping agents derived from the castor plant have been shown to improve surface stability and longer antimicrobial activity [20, 22].

Therefore, the current work focuses on the green synthesis of ZnO nanoparticles using Ricinus communis seed extract at three precursor concentrations (0.01, 0.05 and 0.07 M), their structural, morphological and optical characterization, and their antibacterial activity against Gram-positive and Gram-negative bacteria. In particular, the study examines how the precursor concentration affects the particle size, band gap and antibacterial performance of the ZnO NPs. This work contributes to sustainable nanotechnology and offers a low-cost, biocompatible antimicrobial agent that can be useful in areas like medicine, food preservation and environmental management [7, 12, 18].

2 Materials and Methods

2.1 Synthesis of Nanoparticles

Dehulled and ground seeds (Ricinus communis) were extracted with deionized water at a concentration of 10 g/100 mL. In brief, 10 g of ground seeds was added to 25 mL of water at 60 °C, then diluted to 100 mL and magnetically stirred at 60 °C for an additional 30 min. After cooling, the solution was centrifuged (6000 rpm, 10 min) and filtered through Whatman filter paper to produce a clear aqueous castor seed extract, which served as a green reducing/capping medium.

To synthesize ZnO, zinc acetate solutions (0.01, 0.05 and 0.07 M) were prepared separately, and the castor seed extract was added dropwise under vigorous stirring. The mixture was stirred for 1 h at 60 °C, and the product was centrifuged, washed with ethanol, dried in an oven at 80 °C, and then calcined at 500 °C to obtain crystalline ZnO nanoparticles. The overall biosynthesis procedure is illustrated schematically in Fig. 1.



Fig. 1 Schematic diagram of the biosynthesis steps of ZnO nanoparticles using castor (Ricinus communis)

3 Characterization Techniques

3.1 UV–Vis DRS (Diffuse Reflectance Spectroscopy)

UV–Vis characterization of the as-prepared ZnO NPs was carried out at room temperature. Absorption spectra were measured with a Shimadzu UV-3600 spectrophotometer (Japan, 200–700 nm) and, for selected samples, with a PerkinElmer LAMBDA 365 UV–Vis spectrophotometer (USA, scanning range: 200-900 nm).

3.2 XRD (X-ray Diffraction)

The phase structure and crystallinity of the prepared ZnO nanoparticles were determined by X-ray diffraction (XRD). Measurements were taken at room temperature with a PANalytical X'Pert PRO diffractometer (Malvern PANalytical) outfitted with Bragg-Brentano geometry and Cu Kα radiation (λ = 1.5418 Å). Phase confirmation was carried out by comparing the reflections with those from the ICDD Powder Diffraction File (PDF) database and crystallite size was determined by peak broadening (FWHM), based on the Scherrer equation.

3.3 FTIR (Fourier Transform Infrared Spectroscopy)

Fourier-transform infrared spectroscopy (FTIR) is a vibrational technique that employs a Fourier-transform spectrometer to transform the measured signal into an IR spectrum and provide bands of characteristic frequency (a "fingerprint") that are related to bond vibrations and allow identification of functional groups. FTIR measurements were obtained for samples with a PerkinElmer FT-IR system equipped with the PerkinElmer Spectrum IR software (v10.7.2) in the range 4000–400 cm^{-1} (transmittance, %T).

3.4 TEM (Transmission Electron Microscopy)

The morphology, average particle size and size distribution of the ZnO NPs were analysed by transmission electron microscopy (TEM) using a Carl Zeiss EM10C operated at 100 kV. Samples were prepared by suspending a small quantity of ZnO nanopowder in deionized water and sonicating to obtain a uniform suspension. A drop of the dispersion was placed on a carbon-coated copper TEM grid and air-dried before imaging. Particle size distribution was acquired by measuring particle diameters from many TEM micrographs

and statistically analysing the data with image-analysis software (ImageJ) following standard protocol for TEM nanoparticle sizing.

3.5 FESEM–EDX (Field Emission Scanning Electron Microscopy with Energy Dispersive X-ray)

The morphology and composition of the biosynthesized zinc oxide nanoparticles (ZnO NPs) were investigated using FE-SEM combined with EDS along with elemental mapping. The analyses were conducted on a ZEISS SIGMA VP FE-SEM instrument having an Oxford Instruments EDS system and elemental mapping detector. The samples were sputter-coated with a thin gold layer before imaging. The FE-SEM micrographs were used to observe the particle morphology, surface texture, degree of agglomeration and overall size characteristics of the ZnO nanostructures.

3.6 Antibacterial Activity

The antibacterial activity of the ZnO NPs was evaluated by the agar well diffusion method against Escherichia coli (Gram-negative) and Staphylococcus aureus (Gram-positive). The microbial inoculum was spread over the entire surface of the agar plate. Wells (4–6 mm in diameter) were then punched aseptically with a sterile borer, and 20–100 µL of the ZnO NP suspension at concentrations of 0.375, 0.75, 1.5 and 3 mg/mL was added to each well. The plates were incubated at 37 °C for 24 h, during which the nanoparticles diffused into the agar medium and inhibited the growth of the test strain. The diameter of the inhibition zone (mm) was measured as an indicator of antibacterial activity.

4 Results and Discussion

4.1 UV–Vis

UV–Visible spectra were obtained within the 200–700 nm range at ambient temperature. To ensure consistency in comparing ZnO samples, the spectra underwent baseline correction (using the high-wavelength region), and the optical band gap (E_g) was determined utilizing the Tauc method for a direct allowed transition, through plotting and extrapolating the most linear region to the energy axis [21]. This technique, although widely utilized, necessitates careful selection of the linear segment to avoid systematic errors in E_g determination.

As shown in Figure 2, the castor extract displayed pronounced UV absorption, peaking at $\lambda_{max} \approx 295$ nm, indicating the presence of plant chromophores. Absorption characteristics within the 240–400 nm range in many flavone/flavonol-rich extracts are often attributed to Band II (≈240–280 nm) and Band I (≈300–380 nm), confirming the presence of conjugated aromatic systems and underscoring the role of phytochemicals in green synthesis and surface stabilization.

Table 1 Absorption edge and optical band gap of green-synthesized ZnO nanoparticles

Sample	Concentration (M)	Absorption edge, λ_{edge} (nm)	Optical band gap, E_g (eV, Tauc direct.)	Linear-fit R^2
C1	0.01	379	3.121	0.947
C2	0.05	380	3.115	0.961
C3	0.07	380	3.100	0.976

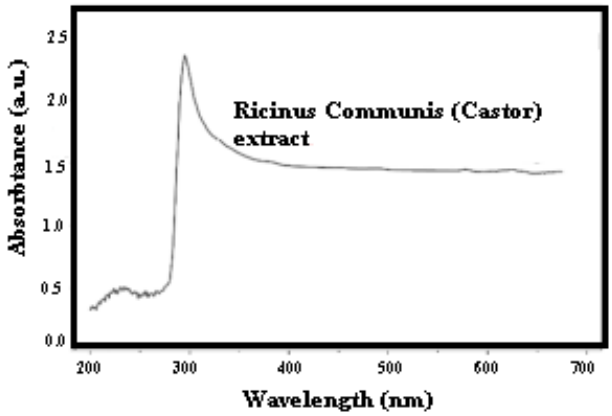


Fig. 2 UV–Vis absorption spectrum of Ricinus communis (castor) extract recorded in the 200–700 nm range

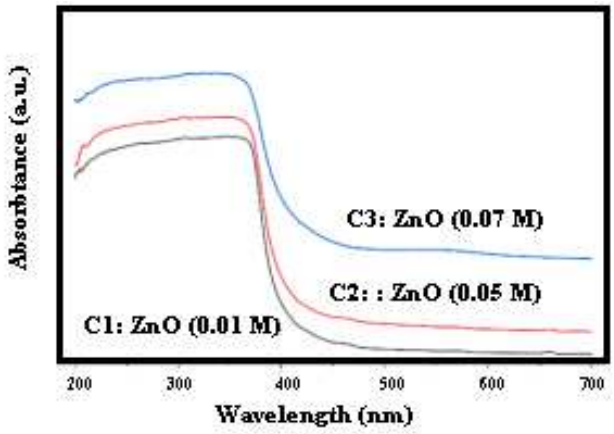


Fig. 3 UV–Vis absorption spectra of green-synthesized ZnO nanoparticles prepared at different precursor concentrations (0.01, 0.05 and 0.07 M) recorded in the 200–700 nm range

All ZnO samples shown in Figure 3 exhibit clear near-band-edge absorption in the UV range, with an absorption onset at approximately 379–380 nm, characteristic of ZnO as a wide, direct band-gap semiconductor. Through direct-transition Tauc analysis, the determined E_g values were 3.121 eV (C1, 0.01 M), 3.115 eV (C2, 0.05 M), and 3.100 eV (C3, 0.07 M) as shown in Table 1, indicating a slight decrease in E_g with increasing precursor concentration under the specified synthesis conditions. When reporting E_g values from UV–Visible measurements, it is crucial to document the fitting region and goodness-of-fit due to potential influences of scattering/aggregation and sub-band-gap absorption that may impact the perceived linearity and E_g determination.

4.2 FTIR

Figure 4 shows the FTIR spectra, which confirm the formation of ZnO NPs and the presence of surface-adsorbed species originating from the green synthesis route. A well-defined absorption peak at 486 cm^{-1} can be assigned to the Zn–O stretching vibrational mode in wurtzite ZnO and it is a typical feature within the range of 450–650 cm^{-1} associated with ZnO-based nanostructures. The main FTIR bands and their assignments are summarized in Table 2.

Table 2 FTIR band assignments for green-synthesized ZnO (from Fig. 4)

Observed band (cm^{-1})	Assignment	Interpretation
~486	Zn–O stretching	Confirms ZnO lattice vibrations
~1626	δ(H–O–H) bending	Adsorbed water on ZnO surface
~3435	O–H stretching	Surface –OH / physically adsorbed water
~1000–1500 (multiple)	C–O / C–N and organic modes; possible carbonate contributions	Residual/capping phytochemicals and/or surface carbonates

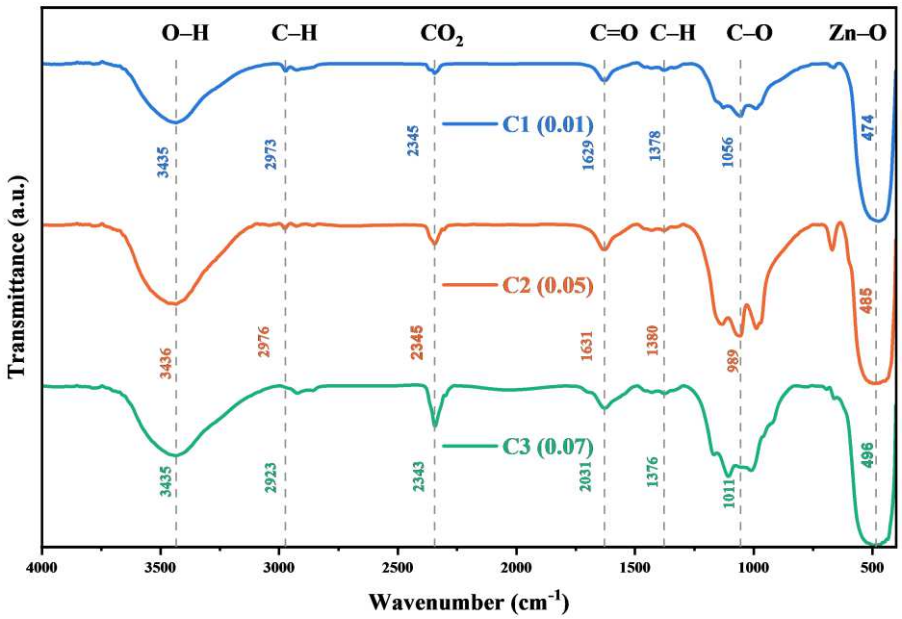


Fig. 4 FTIR spectra of green-synthesized ZnO nanoparticles prepared at various precursor concentrations (C1: 0.01, C2: 0.05 and C3: 0.07 M)

The broad band at 3435 cm^{-1} is assigned to O–H stretching from surface-adsorbed hydroxyls and/or physisorbed water, while a band at 1626 cm^{-1} arises from H–O–H bending (δOH) of adsorbed molecular water. Such hydroxyl/water-related features are commonly visible in oxide nanoparticles because of their large surface area and high affinity for moisture; analogous assignments for bands near 3460 and 1620 cm^{-1} bands are well established in the literature.

Besides the Zn–O and hydroxyl modes, several other bands are present in the fingerprint region (≈1000–1500 cm^{-1}) of the FTIR spectra, corresponding to C–O / C–N stretching and/or organic functional groups from plant extracts in the system that might act as capping/stabilizing ligands during green synthesis. In addition, other types of surface species on metal oxides related to carbonate often occur as two bands in the regions 1250–1400 cm^{-1} (symmetric C–O stretching) and 1500–1600 cm^{-1} (antisymmetric C–O stretching) that vary in overall strength according to surface chemistry and exposure to atmosphere. In general, the three samples exhibit the same set of dominant FTIR

signatures, suggesting similar surface functionalization across concentrations. The differences in band intensity between the spectra are attributed to relative variations in the content of adsorbed species rather than to a change in the ZnO phase.

4.3 XRD

The XRD powder patterns (Figure 5) show well-defined reflections of hexagonal wurtzite ZnO, whose major peaks can be indexed to planes such as (100), (002), (101), (102), (110), (103), (200) and (112), in agreement with the standard reference ZnO pattern from JCPDS/PDF 36-1451. The presence of these indexed peaks and the absence of other intense reflections due to secondary phases (e.g., $Zn(OH)_x$ or other zinc compounds) indicate that the prepared powders are phase-pure ZnO within the detection limits of X-ray powder diffraction.

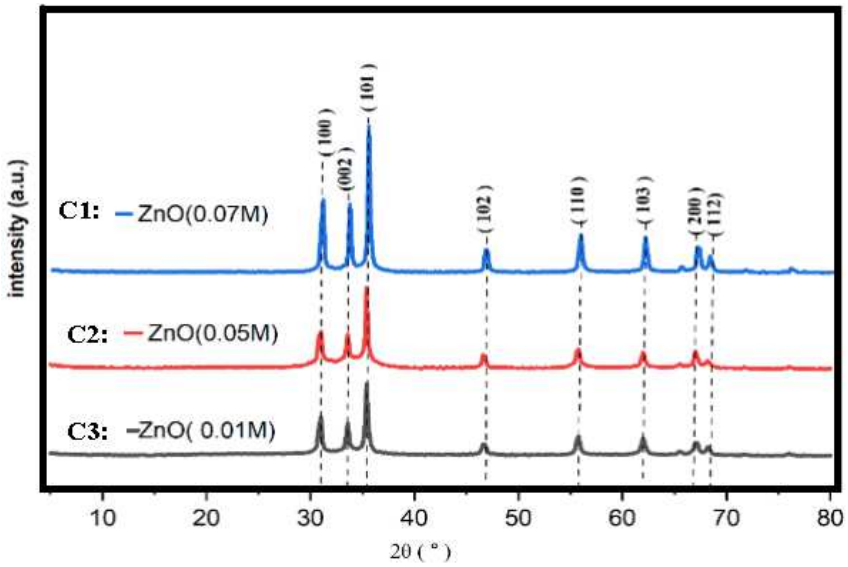


Fig. 5 X-ray diffraction (XRD) patterns of green-synthesized ZnO nanoparticles prepared at different precursor concentrations (C1: 0.01, C2: 0.05 and C3: 0.07 M)

Concentration-dependent changes in diffraction intensity and peak width are evident for the three samples (0.01, 0.05, 0.07 M). In general, sharp and intense peaks indicate enhanced crystallinity and/or a larger coherently diffracting domain size, while broadened peaks are related to smaller crystallite size and micro-strain. For powdered ZnO, the strongest reflection usually corresponds to the (101) plane, and the relative intensities of the main peaks may vary with preferred orientation and growth kinetics as the precursor concentration changes under otherwise identical synthesis conditions.

4.4 TEM

Figure 6 (A–F) shows the TEM micrographs and particle size distribution histograms of green-synthesized ZnO nanoparticles prepared at different precursor concentrations: C1 (0.01 M), C2 (0.05 M) and C3 (0.07 M). In the TEM images, the nanoparticles are partly agglomerated and locally overlap one another rather than appearing as completely separate particles, which is typical behavior of ZnO nanoparticles. Quantitatively, the measured sizes exhibit an increase with increasing concentration: C1 (0.01 M) gave $\mu = 27.58$ nm, $\sigma = 7.90$ nm ($n = 55$); C2 (0.05 M) yielded $\mu = 36.50$ nm, $\sigma = 9.39$ nm ($n = 45$); and C3 (0.07 M) showed the largest size and broadest distribution, with $\mu = 53.64$ nm, $\sigma = 15.14$ nm ($n = 28$), indicating increased polydispersity compared with the lower concentrations. The

aforementioned tendency toward a progressively larger particle size at higher precursor concentration is in agreement with reports that precursor concentration can strongly affect the growth and final size distribution of ZnO nanoparticles. The mean size of C1 is also close to the ≈27 nm reported for algae-mediated ZnO NPs [16].

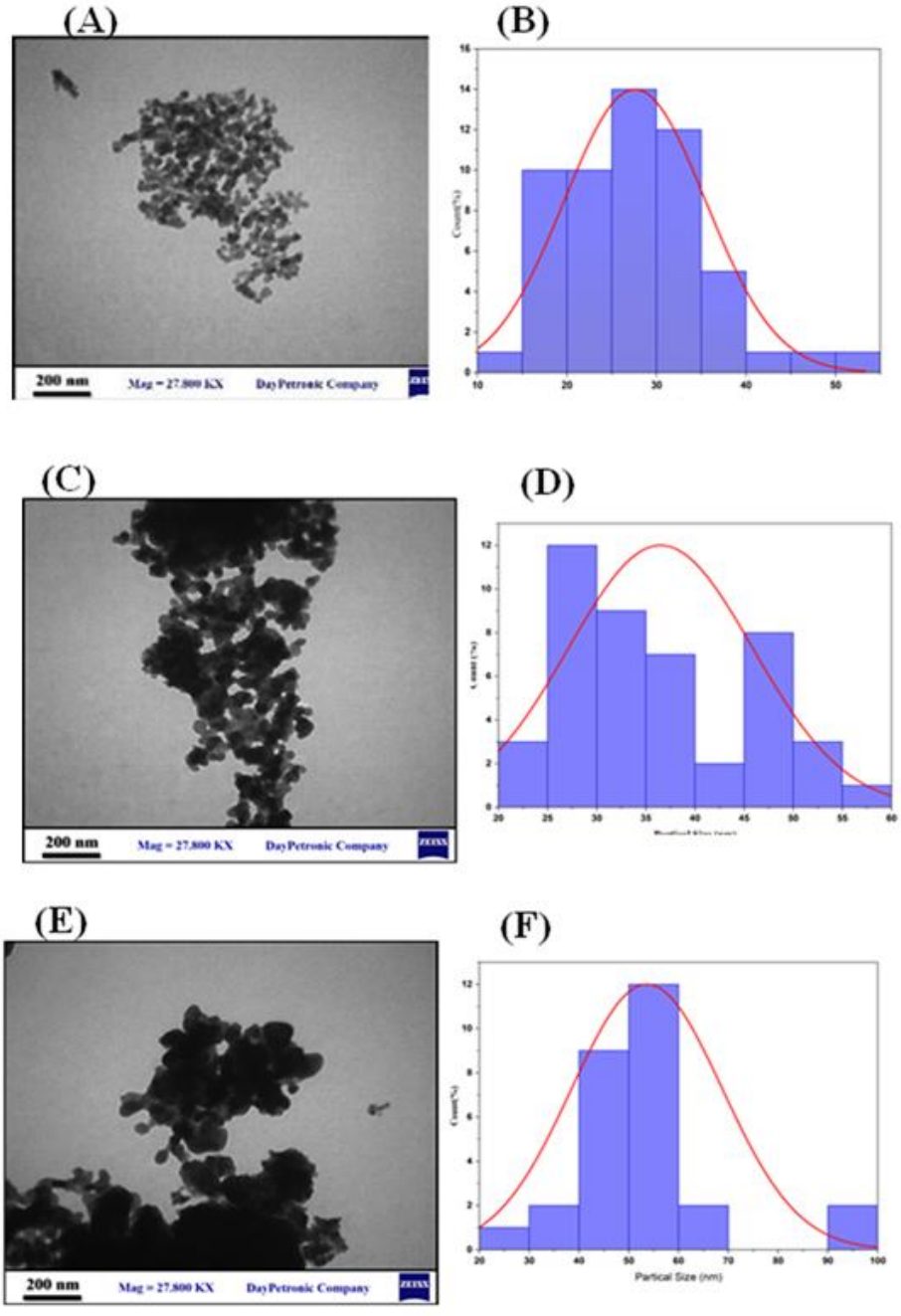


Fig. 6 TEM micrographs and particle size distribution histograms of biosynthesized ZnO nanoparticles: (A, C, E) TEM images; (B, D, F) corresponding particle size distribution (PSD) histograms with Gaussian fitting

4.5 FE-SEM

As shown in Figure 7, the biosynthesized ZnO samples (C1–C3) consist of nanoscale crystallites that form dense clusters rather than free-standing particles. This morphology is

commonly found in ZnO nanomaterials. Owing to their high surface energy, the nanoparticles tend to pack into relatively large assemblies during drying or subsequent processing, regardless of whether they are covered by biomolecules from plant-derived sources.

The surface texture of all three samples appears granular and heterogeneous, with many smaller primary particles clustering together to form agglomerates. This kind of aggregation is consistent with plant-mediated routes, where phytochemicals may act as reducing or capping agents. However, after calcination, the particles in the final powder remain in contact (van der Waals interactions and necking), forming aggregates of non-uniform size. This type of overall morphology is consistent with successful generation of nanostructured ZnO, and also reflects the inherent tendency of ZnO nanoparticles to assemble into secondary particles.

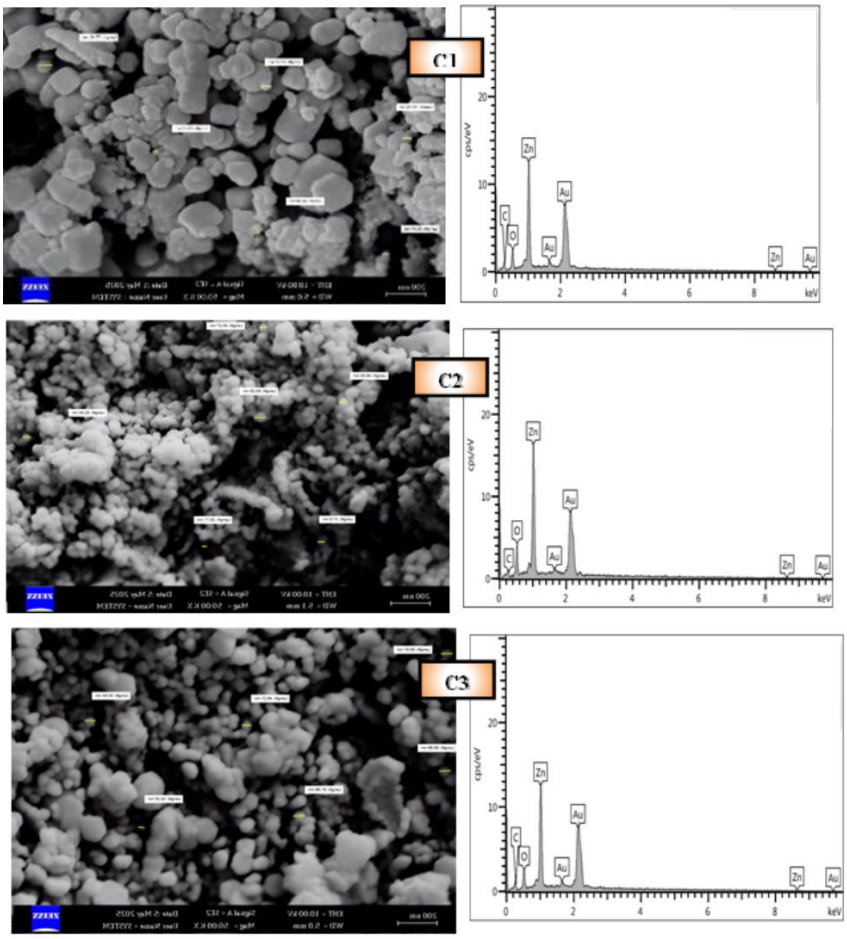


Fig. 7 FE-SEM micrographs and corresponding EDS spectra of green-synthesized ZnO nanoparticles prepared at various precursor concentrations: C1 (0.01 M), C2 (0.05 M) and C3 (0.07 M)

Table 3 Elemental composition (wt%) of ZnO nanoparticles estimated from EDS analysis

Sample	Concentration	Zn (wt%)	O (wt%)	C (wt%)
C1	0.01	83.1	10.8	6.1
C2	0.05	82.6	12.0	5.4
C3	0.07	83.2	9.7	7.1

The EDS results (Table 3) confirm that Zn and O are the dominant elements in all samples, which supports the formation of ZnO. Small carbon signals were also detected, likely originating from residual organic species involved in plant-derived capping and/or from the carbon adhesive tape used to mount the samples.

In addition, the Au peaks visible in the spectra are consistent with the conductive sputter coating used for SEM imaging of non-conductive or weakly conductive samples. Gold coating is widely applied to reduce charging and improve image quality, but it also introduces Au X-ray lines in the EDS spectra; therefore, Au is interpreted as a preparation artifact rather than a constituent element of ZnO.

4.6 Antibacterial Activity

The antibacterial effect of the ZnO nanoparticle suspensions against E. coli was clearly concentration-dependent (Figures 8, 9). No measurable zones of inhibition were observed at the lowest doses (0.375–0.75 mg/mL), while large zones of inhibition developed at higher doses, measuring 13–16 mm at 1.5 mg/mL and 20–22 mm at 3 mg/mL. This trend is consistent with the known dose-dependence of the antibacterial efficacy of ZnO NPs, which increases with the effective mass and availability of NPs at the diffusion front. The maximum zones obtained here (20–22 mm at 3 mg/mL) are comparable to the 21.2 mm reported against E. coli for actinomycete-mediated ZnO NPs at 5 mg/mL [3] and larger than the 12.3 mm reported for Tetraselmis indica-mediated ZnO NPs [16].

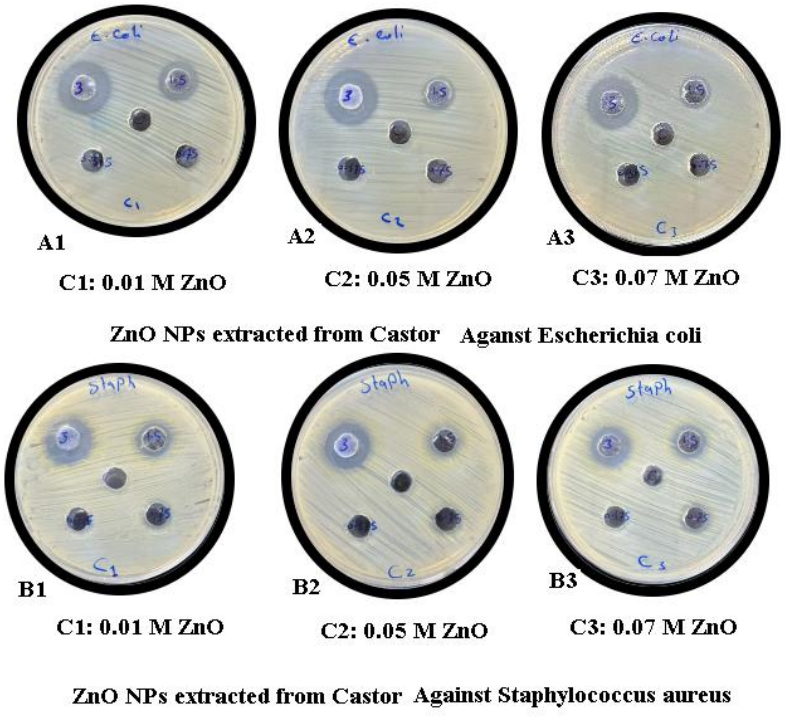


Fig. 8 Representative agar well diffusion plates showing the antibacterial activity of green-synthesized ZnO nanoparticles against Escherichia coli (A1–A3) and Staphylococcus aureus (B1–B3) at different precursor concentrations (C1–C3)

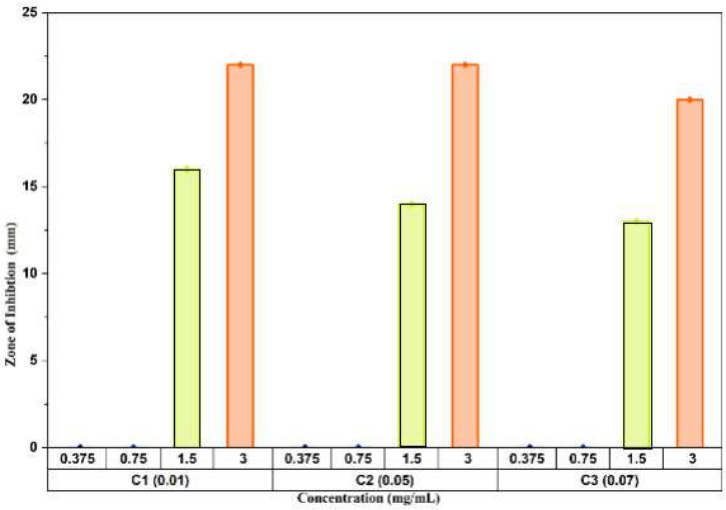


Fig. 9 Dose-dependent antibacterial activity of green-synthesized ZnO nanoparticles (C1–C3) against Escherichia coli, expressed as zone of inhibition (mm) determined by the agar well diffusion method at different ZnO concentrations (mg/mL)

A dose-response was also observed for S. aureus (Figure 10), with larger inhibition zones at higher ZnO doses. Unlike in E. coli, inhibition starts at lower concentrations for some of the samples (≈0.75 mg/mL); and the zones generally reach ~17–20 mm at 3 mg/mL. This is in agreement with several ZnO-NP studies that have reported a strong effect on Gram-positive bacteria, which has been associated with differences in cell-envelope architecture and in susceptibility to oxidative and membrane-disruptive stress between Gram-positive and Gram-negative bacteria. Comparable inhibition zones against S. aureus have been reported for other biogenic ZnO NPs, e.g., 18.4 mm for T. indica-mediated ZnO [16] and 22.8 mm at 5 mg/mL for actinomycete-mediated ZnO [3].

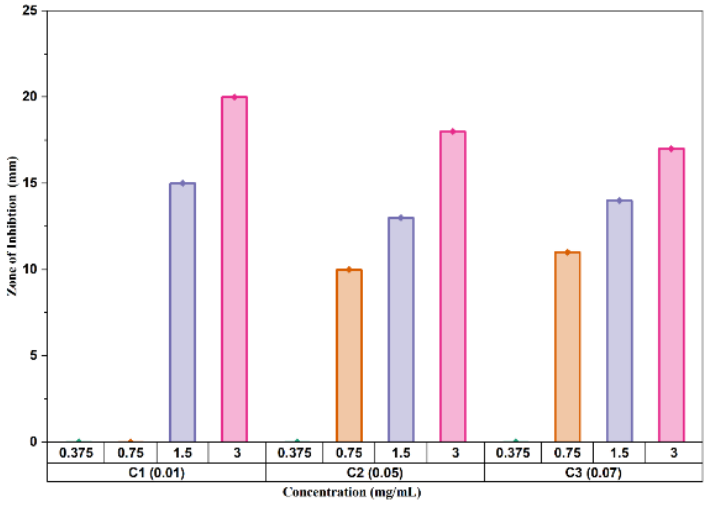


Fig. 10 Dose-dependent antibacterial activity of green-synthesized ZnO nanoparticles (C1–C3) against Staphylococcus aureus, expressed as zone of inhibition (mm) determined by the agar well diffusion method at different ZnO concentrations (mg/mL)

4.6.1 Comparative performance of C1–C3

For both organisms, the inhibition zones show that antibacterial activity is a function of ZnO dose (mg/mL) and also depends on the synthesis condition, i.e., the precursor

concentration (C1–C3). C1 generally yields higher zones at the higher concentrations (especially at 3 mg/mL), implying more effective antibacterial action under those synthesis conditions (e.g., due to differences in surface chemistry, defect density or dispersion/aggregation state that affect contact killing and diffusion). This is consistent with the smaller particle size of C1 (≈27.6 nm, Fig. 6), which provides a larger specific surface area for interaction with bacterial cells. However, particle size is not the only factor, since Zn^{2+} ion release and surface properties have also been shown to strongly influence the antibacterial effect of ZnO [24]. The most frequently described mechanisms of ZnO NP action are the production of reactive oxygen species (ROS), the release of Zn^{2+} ions, and physical damage to the cell membrane, leading to leakage of cellular contents and loss of cell viability.

Well diffusion provides a convenient and standardized relative measure of antibacterial activity in terms of inhibition-zone diameter (mm); however, the zone size depends on diffusion through the agar as well as on intrinsic potency. Therefore, the dose–response trends and the relative ranking of C1–C3 should be regarded as semi-quantitative comparisons under identical experimental conditions.

5 Conclusion

The Ricinus communis (castor) extract-mediated green synthesis of ZnO NPs provided an eco-friendly and low-cost alternative to conventional methods that use harsh reagents and conditions. The plant-based strategy is attractive because phytochemicals can assist particle growth and surface stabilization.

The characterization confirmed the formation of ZnO and showed precursor-concentration-dependent properties. XRD confirmed the hexagonal wurtzite structure of ZnO, while FTIR indicated the Zn–O vibration (486 cm^{-1}) as well as bands indicating surface hydroxyl/ adsorbed water (3435 and ∼1626 cm^{-1}), also observed on oxide nanoparticle surfaces. UV–Vis spectra showed the characteristic near-UV absorption edge of ZnO, with the band gap decreasing slightly from 3.121 to 3.100 eV as the precursor concentration increased; TEM and FE-SEM confirmed the formation of agglomerated nanoparticles, with mean TEM sizes increasing from 27.6 to 53.6 nm. Together, these results show that the green route provides ZnO crystallites with surface functionalities of relevance in stability and biological interaction.

The ZnO NPs showed dose-dependent antibacterial activity against both E. coli and S. aureus, with inhibition zones of up to about 22 mm and 20 mm, respectively, at 3 mg/mL. The C1 sample, which had the smallest particle size, generally produced the largest inhibition zones. These findings suggest that castor-mediated ZnO NPs are promising candidates for antimicrobial applications.

Declarations

Funding. The authors declare that no funds, grants, or other support were received during the preparation of this manuscript.

Competing interests. The authors have no relevant financial or non-financial interests to disclose.

Ethics approval. Not applicable. This study did not involve human participants or animals.

Consent to participate. Not applicable.

Consent for publication. Not applicable.

Data availability. The data supporting the findings of this study are available from the corresponding author upon reasonable request.

Author contributions. Mohanad Ghulam Murad Alzubaidi: conceptualization, methodology, investigation, formal analysis, writing – original draft. Ali Bahari: supervision, conceptualization, writing: supervision, validation, writing – review and editing. All authors read and approved the final manuscript.

References

[1] Al-Darwesh, M.Y., et al.: A review on plant extract mediated green synthesis of zinc oxide nanoparticles and their subsequent biomedical use. Mater. Today Commun. 37, 104439 (2024)

[2] Gul, A., et al.: Green synthesis, characterization, enzyme inhibition and antioxidant potential of silver nanoparticles derived from leaf and root extracts of natural plants. Int. J. Nanomed. 16, 511–524 (2021)

[3] Rajkumari, R., Nishikanta, A., Chanu, K.L., et al.: Microbial nanobiotechnological approach of actinomycete-mediated zinc-oxide nanoparticle biosynthesis: Taguchi experimental design, characterization, antimicrobial properties and its early growth responses in rice. BioNanoScience 16, 724 (2026). https://doi.org/10.1007/s12668-026-02964-0

[4] Shobha, N., Prakash, S.: Synthesis and characterisation of zinc oxide nanoparticles by solution combustion technique. Mater. Sci. Eng. C 101, 124–133 (2019)

[5] Arif, R., Uddin, R.: Recent developments in biosynthesis of silver nanoparticles. Med. Devices Sens. 4, e10158 (2021)

[6] Anand, U., et al.: Safer plant-based nanoparticles for combating antibiotic resistance. Sci. Total Environ. 838, 155929–39 (2022)

[7] Hayat, M., et al.: Phytogenic-mediated ZnO nanoparticles using seed extract. ACS Omega 9(20), 13536–13546 (2024)

[8] Mensah, M.B., Awudza, J.A.M., O'Brien, P.: Castor oil: a suitable green source of capping agent for nanoparticle syntheses and facile surface functionalization. R. Soc. Open Sci. 5(8), 180824 (2018)

[9] Mubofu, E.B.: Castor oil as a potential renewable resource for functional materials. Sustain. Chem. Process. 4, 5 (2016)

[10] Soni, N., Dhiman, R.C.: Phytochemical, antioxidant, and antimicrobial activity of Ricinus communis synthesized silver nanoparticles. Chin. Herb. Med. 9(3), 289–294 (2017)

[11] Ramothloa, T.P., et al.: Phytochemical composition and multifunctional activities of Ricinus communis: a review. Molecules 30, 3214 (2025)

[12] Waris, M., et al.: Evaluation of larvicidal efficacy of Ricinus communis extracts and nanoparticles. Parasites Vectors 13, 426–436 (2020)

[13] Bouttier-Figueroa, D.C., Cortez-Valadez, M., Flores-Acosta, M., Robles-Zepeda, R.E.: Green synthesis of zinc oxide nanoparticles using plant extracts and their antimicrobial activity. BioNanoScience 14(3), 3385–3400 (2024). https://doi.org/10.1007/s12668-024-01471-4

[14] Okaiyeto, I., et al.: Biogenic ZnO nanoparticles as promising antibacterial agents. Int. J. Mol. Sci. 25, 9500–510 (2024)

[15] Mahendiran, D., Subash, G., Arumai Selvan, D., Rehana, D., Senthil Kumar, R., Rahiman, A.K.: Biosynthesis of zinc oxide nanoparticles using plant extracts of Aloe vera and Hibiscus sabdariffa: phytochemical, antibacterial, antioxidant and anti-proliferative studies. BioNanoScience 7(3), 530–545 (2017). https://doi.org/10.1007/s12668-017-0418-y

[16] Thirumoorthy, G.S., Balasubramaniam, O., Kumaresan, P., Muthusamy, P., Subramani, K.: Tetraselmis indica mediated green synthesis of zinc oxide (ZnO) nanoparticles and evaluating its antibacterial, antioxidant, and hemolytic activity. BioNanoScience 11(1), 172–181 (2021). https://doi.org/10.1007/s12668-020-00817-y

[17] Ali, J., et al.: Green-based approach to synthesize silver nanoparticles using Penicillium oxalicum. ACS Omega 7, 46653–46673 (2022)

[18] Lule, S., Sequeira, S.K.: Metal nanoparticles of microbial origin and their antimicrobial applications. In: Nanotechnological Approaches in Food Microbiology. CRC Press, Boca Raton (2020)

[19] Huq, A., et al.: Green synthesis and potential antibacterial applications of bioactive silver nanoparticles. Polymers 14(4), 742 (2022)

[20] Ogaidi, A., Al-Jobori, K.M., Ghareeb, A.M.: Green synthesis of Ag NPs by Ricinus communis extract and investigation of antibacterial potential. J. Genet. Eng. Biotechnol. 19, 44 (2021)

[21] Akhtari, N., et al.: Antioxidant and antimicrobial properties of ZnO NPs green synthesized with essential oils. Sci. Rep. 15, 12117 (2025)

[22] Singh, R.K., et al.: Plant-based nanoparticles as new antimicrobial agents. J. Biol. Inorg. Chem. 30(8), 1325–1344 (2024)

[23] Linima, V.K., et al.: Biogenic synthesis of Ricinus communis mediated iron and silver nanoparticles. Int. J. Nanomed. Res. 14(2), 133–144 (2023)

[24] Quintero García, O.J., Pérez Soler, H., Bobadilla Barrón, G., Sánchez Carbente, M.R., Amezcua Allieri, M.A., Olvera Amador, M.L.: Influence of commercial ZnO particle size on the inactivation of Escherichia coli DH5α. BioNanoScience 16(2), 96 (2026). https://doi.org/10.1007/s12668-025-02294-7